TBI INDUCED RATE DEPENDENT VISCOELASTIC RESPONSE OF AXON: PREDICTIONS FROM A MATHEMATICAL MODEL

by

MANIKANTA JONNALAGADDA

Presented to the Faculty of the Graduate School of

The University of Texas at Arlington in Partial Fulfillment

of the Requirements

for the Degree of

MASTER OF SCIENCE IN AEROSPACE ENGINEERING

THE UNIVERSITY OF TEXAS AT ARLINGTON

December 2015

Acknowledgements

I would like to extend my sincere gratitude to Dr. Ashfaq Adnan for his guidance and support during the whole span of this study as my Project Supervisor. It was a pleasure to work with him who shared a passion for the subject and provided valuable suggestions even during the busiest hours. I am sure; he would remain an inspiration to me for the years to come.

I would like to thank Dr. Kent Lawrence and Dr. Wen Chan for their accessibility and being members on my dissertation committee, besides providing me with wealth of knowledge in the coursework. I would like to thank all teaching and administrative faculty in MAE, for delivering your best and making my journey at UTA.as smooth as it could be.

I appreciate all my group mates at MMPL lab who provided exceptional ideas and constructive criticism which mattered a lot. It was a great bunch of people who maintained great healthy atmosphere.

Finally endless thanks to my family and friends for their support and encouragement without which I would have never reached this stage.

November 20, 2015

Abstract

TBI INDUCED RATE DEPENDENT VISCOELASTIC RESPONSE OF AXON:

PREDICTIONS FROM A MATHEMATICAL MODEL

Manikanta Jonnalagadda, MS

The University of Texas at Arlington, 2015

Supervising Professor: Name Ashfaq Adnan

Traumatic brain injury (TBI) accounts to almost one fifth of total fatal injuries. Even though there are various mechanisms hypothesized for the causes leading to TBI, diffuse axonal injury (DAI) is found to be the most observed criterion. The reason for axonal failure in DAI has been studied extensively using experimental and computational models. It was found that axons behave like viscoelastic materials, thus exhibiting rate dependent behavior under loading. This viscoelastic behavior of axons is believed to drive the failure of axons and its substructures. It was observed that axon failure is caused by failures and distortions in axonal cytoskeleton, particularly Microtubule-Tau protein assembly.Inspired by the previous work, we have developed modified shear lag model to predict axonal damage under dynamic loading conditions.

Opposed to previous work where only tau proteins were considered viscoelastic, we have assumed both microtubules and tau proteins to be viscoelastic and modeled them using a two parameter kelvin model. We have then studied the effect of strain rate on viscoelastic response of microtubule –tau protein assembly. We have attempted to determine a phase diagram in terms of loading rate and applied strain to isolate the two possible axonal deformation modes, namely microtubule failure due to excessive stretch and reversible microtubule sliding due to tau protein stretch

Table of Contents

List of Illustrations

List of Tables

Chapter 1

Introduction

1.1 TBI Epidemiology

TBI (Traumatic Brain Injury) is a rapidly growing health problem in United States. Normal brain functioning is disrupted as a result and may lead to death or some kind of severe disability. The cause can be a blow or penetrating head injury or an explosive blast. Centers for Disease Control and Prevention (CDC) statistics of 2010 suggest about 2.5 million cases of TBI were checked at emergency department (ED) across United States (Frieden, Houry, & Baldwin, 2014). Of these about 2% or 53000 of the people died. But CDC reports that number of people experiencing TBI may be higher as the above reported numbers does not include those who never received medical attention to this or those who are treated at military hospitals. Military personnel are more susceptible to TBI now days as a result of the improvised explosive devices (IED's) used in the modern day war environment. Department of Defense (DOD) statistics reveal that in the last decade (from 2000 through 2011) 4.2% of the serving army personnel suffered (Frieden, Houry, & Baldwin, 2014)

1.2 Social Impact

TBI adversely affects a person's life in multiple ways which affect social and occupational functioning. In addition to the person suffering, it adversely impacts families, communities and the economy. It was found that adults discharged from rehabilitation centers after moderate or severe TBI were twice more likely than others to die in the 3.5 years following injury. Other chronic effects are also seen in people of various ages following injury treatment and rehabilitation.

Elderly people aged more than 75 are more likely to suffer TBI. Statistics suggest that among the non-fatal TBI falls with 35% contribute the most cases, followed by motor

vehicle crash (MVC) injuries amounting 17%, blows or impact to head during sports etc., amounting to 17%. Leading causes of TBI related ED is shown in the table 1-1

Table 1-1 Estimates of Average annual numbers of TBI during 2002 -2010 [6]

Mechanism of Injury	***ED visits***	***Hospitalizations***	***Deaths***
Falls	658,668	66,291	10,944
Struck by or against an object	304,797	6,808	372
Motor vehicle traffic	232,240	53,391	14,795
Assault/Homicide	179,408	15,032	5,665

Chapter 2

Literature Review

2.1 Definition of TBI

Any damage resulting from mechanical loading to head is called Traumatic Brain Injury (TBI). It's generally caused during falls, motor vehicle crashes, explosions and sports accidents. Traumatic injury is one of those greatest disorders caused due to mechanical loading to neural system. Particularly brain injury which is the most common cause for many traumatic injury deaths and sufferings has led to the primary and early focus in the study of brain mechanics. Penetration, impacts and acceleration-deceleration are the general criterion used to differentiate the injury on macro scale, as seen in the figure 2-1 (Zink & McQuillan, pp. 36-43) The amount of force applied, its orientation and site of application determines the amount of damage. During the loading process which occurs over milliseconds results in abnormally excessive accelerations (Davis, 2000). Pathological features seen depend on these mentioned factors. For example hemorrhages and tissue lesions are often seen in the contact or penetration injuries, whereas diffuse axonal injury (DAI) is observed in cases related to rapid head acceleration-deceleration. TBI due to its nature of invoking irreversible and chronic health effects is termed as a disease process rather than a discrete event

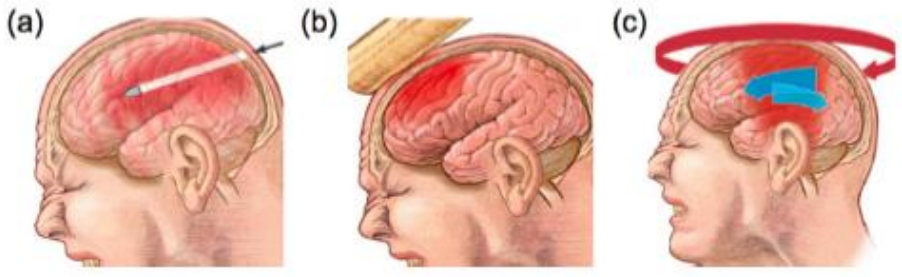

Figure 2-1 TBI Mechanisms. (a) penetrating injury (b) contact injury (c) acceleration-deceleration injury[25].

2.2 Brain Structure

Brain structure is the main reason for its susceptibility to traumatic brain injury. The outer layer of the cerebrum (brain) is cortex and it is protected by rigid skull. Membranous layers like dura mater, arachnoid and pia mater are present in between the skull and brain. Cerebral spinal fluid flowing between the arachnoid and pia mater serves to protect brain. CSF helps to dampen the impact forces experienced by the head. Brain almost floats in the CSF inside the skull. It is connected to or supported by skull by means of parasagittal bridging veins, cranial nerves, tentorium and parasinusoidal granulations (Reilly & Bullock, 1998). Dura mater contains stiff membranes like falx cerebri and tentorium cerebelli which extend into cortex and provide resistance to brain movements, when subjected to inertial loading. As shown in figure 2-2 (Wright, 2012), superior right and left cerebral hemispheres are partially separated by falx cerebri which extends vertically into cortex whereas occipital lobes of brain are separated from cerebellum by the tentorium cerebelli.

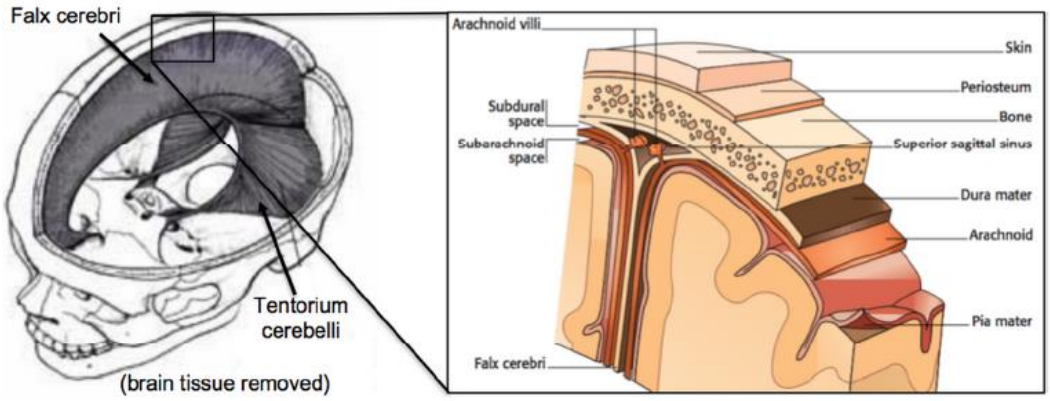

Figure 2-2 Membrane layers surrounding the brain tissue [24]

Brain tissue contains neurons (nerve cells), supporting cells (astrocytes, glia) and cerebral vasculature system. Neurons are the functional units of the brain and there are

about 100 billion of them present in the normal human brain. Neurons through axons transmit the information in the form of electrical signals. Axons diameter is of few microns but they can be as long as several centimeters. Excess ions and neurotransmitters are removed from extra cellular space by glial cells apart from regulating the blood flow. Cerebral vasculature helps in transport of oxygen and nutrients to brain cells.

Brain tissue discussed above can be differentiated into white and grey matter. Cell bodies and unmyelinated axons are present in the grey matter, whereas white matter contains myelinated axons bundled into neural tracts. The neural tracts by connecting different regions serve as means of communication between different regions of the brain. White color is due to the myelinated sheath (helps in insulating and faster transmission of electric signals) produced by oligodendrocytes present around axons. Organized arrangement of axons in white matter leads to anisotropic behavior of white matter, whereas grey matter is considered an isotropic material

Brain is often visualized in one of the three standard anatomical planes as shown in figure 2-3. They are the coronal plane, the axial plane and the sagittal plane. The coronal plane is vertical and divides anterior and posterior (front and back) sections of the head. The axial plane is horizontal and divides superior and inferior (top and bottom) sections of the head. The sagittal plane is vertical and divides left and right sections of the head

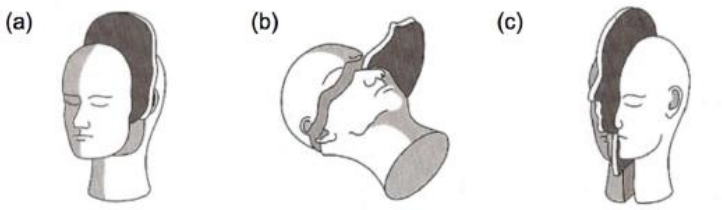

Figure 2-3 Standard Anatomical planes. (a) The coronal plane. (b) The axial plane. (c) The sagittal plane[24].

Brain is divided into left and right hemispheres, brainstem and the cerebellum. Brainstem is composed of medulla, pons and midbrain. Corpus callosum a thick white matter bundle joins the two hemispheres. Ventricles are the fluid filled spaces located deep inside the brain, where cerebrospinal fluid which surrounds the brain and protects it is produced. This structural arrangement is shown in figure 2-4 (Lewis, 2015).

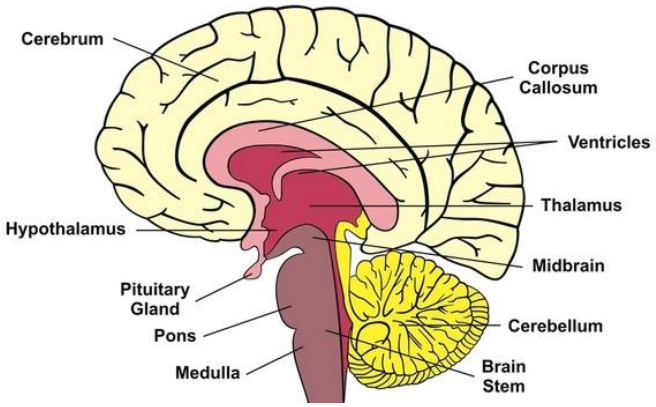

Figure 2-4 Brain Structural arrangement shown in mid sagittal plane [10]

2.3 Biomechanics of Brain Injury

Mechanical load and its consequences to the skull and human brain constitute the bio mechanics of the injury. Impact, impulsive and static loads are the three types of loads experienced based on the load application duration.

Impact loading is where direct contact of skull occurs with object, and loading to head occurs over duration of less than 50ms but usually with a higher magnitude. Contact forces result in ripples of stress waves through brain (Gennarelli, 1992). Based on the state of brain i.e., stationary or in motion at the time of loading brain movement and tissue deformation occur. Local or remote fractures in skull due to contact forces are observed in this type of loading

Impulse loading is due to the indirect loading on head experienced as in cases of bodily impact to steering wheel in vehicular accidents. Here inertial forces set head in

motion even after body comes to rest. It normally occurs over a time range of 50 to 200 ms, and no skull deformation occurs generally due to absence of direct impact. Compressive forces to head causes static loading occurs over longer duration i.e., more than 200 ms and often results in skull fracture or deformation (Gennarelli, 1992).

Inertia force is directly proportional to acceleration for rigid objects. But in dynamic loading, where effects of applied force vary over time, damage to tissue depends on displacement, velocity and acceleration changes. More specifically displacement, velocity, acceleration and its rate dictate the effects on the tissue. Motion of head along the straight line causes translational acceleration as shown in figure 2-5 (Stalhammar, 1990), during which intracranial pressure increases, at point opposite to area of contact, producing negative pressure gradients and thus cavitational bubbles. Brain injury occurs here due to stress waves produced on impact, cavitaional bubble collapse.

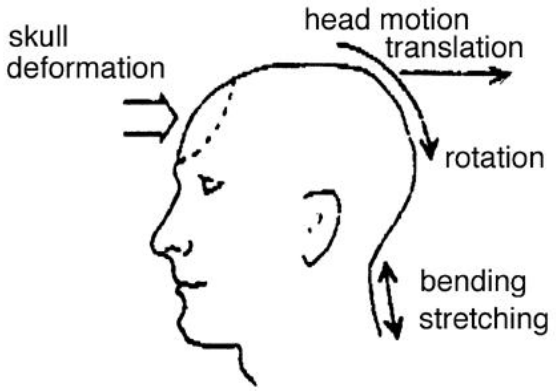

Figure 2-5 Motion of head resulting from impact forces [18]

Turning of head about coronal plane causes rotational acceleration during which brain lags behind skull resulting in tissue strains and intracranial motion. In the dura mater which experiences stress at connections between brain and skull. Bending stretching movement a result of acceleration causes brain stem injury at craniospinal

junction. The most critical acceleration case is when the head experiences accelerations about sagittal plane as shown in figure 2-6 (Smith & Meaney, 2000) and results in diffuse axonal injury (DAI) observed in most brain injuries

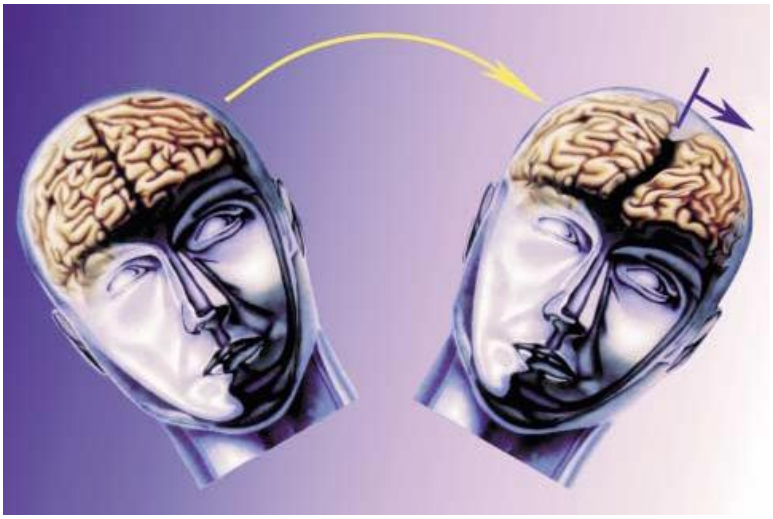

Figure 2-6 Demonstration of DAI resulting from inertial forces [16].

The skull/brain structure exerts counterforce upon the application of mechanical forces. Combined characteristics such as mass, density, elastic and viscous properties of skull/brain resist the forces and help in limiting the magnitude of the forces. Scalp helps in distribution of the impact force through dermal and subcutaneous layers. Skull bone (consisting of two layers, compact bone and spongy layer) contributes to resisting impact force. This shows the protective mechanisms in place naturally, but there are limitations due to skull anatomy. These limitations are primarily due to the skull bone structure which is not as thick at the base and relatively not smooth. This leads to damage to soft viscoelastic brain tissue very easily during impact and to and fro motion across rough internal surfaces. (Stalhammar, 1990)

2.4 Classification of TBI

TBI classification is significant in terms of diagnosis to ensure appropriate treatment is provided. Direct and indirect damage at point of injury lasts for time ranging from hours to weeks, results in brain injury characteristics such as structural failure and neurologic dysfunction. Mechanical and physiologic response of tissue is determined by area of contact and available energy. As discussed earlier these forces lead to several types of head acceleration or movements. Due to this complex mechanism involved, TBIs are classified in numerous ways, like onset time, injury location, pathophysiological response etc. Most often, these injuries belong to more than one category.

Injuries can be classified based on time into two categories, primary and secondary injuries.

2.4.1 Primary Injury

Immediately following impact in a TBI, a primary brain injury occurs resulting from mechanical trauma. Skull fractures, focal injuries, penetrating and diffuse injuries constitute primary injury. Often these mentioned injuries occur simultaneously but one of them predominates. Skull deformations resulting from impact forces either at the site of impact directly or at a remote site indirectly, leads to fractures, epidural hematomas and contusions. During the blunt impact, skull is bent inward at the point of loading resulting in outward bend in the surrounding area. This leads to tensile stress on the skull, and on exceeding the tensile stress limits, fracture occurs and propagates along least resistance path i.e. thinner parts of skull. Depending on the nature of the fracture, they are classified as depressed, linear or basilar. Primary injuries can be distinguished into focal and diffuse injuries based on extent of injury.

2.4.1.1 Focal Injury

Focal injury is a primary injury resulting from blow to head at impact site. Contusions (or bruises) are normally seen in focal injuries. Translational and rotational mechanisms discussed earlier result in contusions. Two main reasons for contusions are bone bent inward stressing the neuronal tissue and released bone causing tensile strain. Severe contusions are often seen in frontal and temporal lobes. Contusions are of two types surface contusions and gliding contusions. Surface contusions are focal injuries and include coup, contrecoup, fracture and herniation contusions. Coup contusions occur at impact site whereas contrecoup contusions occur directly opposite to impact site. Fracture contusion lies underneath the fracture site of skull. Gliding contusions result from rotational motion and are often found in the parasagittal regions where brain is more attached to dura. It is associated to diffuse axonal injury (DAI). Penetrating injuries also come under primary injury and mostly result from ballistic force.

2.4.1.2 Diffuse Brain Injury

Diffuse Axonal injury (DAI) occurs in most cases of Traumatic Brain Injury. As the name suggests, the problem affects axons, which are prone to failure under mechanical loading to the brain. The medical implications are from transport interruption, mechanical breakage of axonal cytoskeleton. Immediate unconsciousness, or confusion are commonly seen in severe TBI, but it was recently found that axon degeneration continues to exist years after injury. Diagnosis of DAI through conventional noninvasive techniques such as CT or MRI is not available as damage occurs at microscopic level.

DAI occurs due to rotational acceleration or deceleration of the head, which result in brain tissue experiencing shearing. Due to the comparatively low shear modulus, brain tissue can shear relatively easily but as it’s confined in the closed skull, it doesn’t have much space to undergo volume deformation. These extremely low shear

deformations cause neuronal axons to stretch at cellular level as shown in figure 2-7 (Wright, 2012). The magnitude of tensile stretch depends on location and orientation of axons. Axons located at the regions of tissue stiffness change are highly vulnerable.to DAI. White and grey matter interfaces, corpus callosum, falx cerebri and tentorium cerebelli where brain motions are restricted during inertial loading result in injury scenarios at the cellular level adjacent to membranes (Smith & Meaney, 2000). Even though DAI occur often in impulsive loading, this can occur during impact loading as well where the contact forces may cause rapid acceleration / deceleration to the brain. The other mechanism is the inertial forces experienced during impulsive loading culminating in impact during motor vehicle crashes. Thus contact forces also are responsible for DAI.

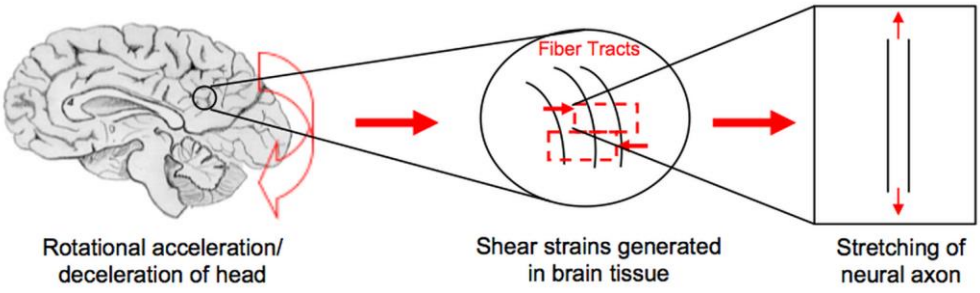

2-7 Acceleration /Deceleration leading to shearing in brain tissue which result in stretching of axons [24]

2.4.2 Secondary Injury

Secondary damage results from the processes initiated by the primary damage, and can last over hours and weeks. Primary traumatic brain injury is made worse due to secondary mechanisms occurring after the mechanical insult. Secondary brain injury can be said to be caused by the anomalies related to primary brain injury such as inflammation, cell receptor mediated dysfunction, etc. Inflammation is normally related to the repair mechanism after injury, but may also result in secondary injury.

2.5 Blast Injury Mechanism

Blast injury scenario is one where a person experiences impact mechanism due to shock wave impact at high velocity, impulsive loading to head almost simultaneously. Explosives upon detonation undergo rapid chemical transformation into gases and releasing large amount of energy. Explosions of conventional explosives results in vigorously expanding gases that occupy 10000 times greater volume than the explosive in addition to the solid residues and shrapnel packed into it. Nuclear detonations result in release of radioactive particles. Generally explosives are measured in strength based on amount of it required to cause damage equivalent to TNT (Stuhmiller, Phillips, & Richmond, 1991). Conventional explosives are in the range of few ounces to thousands of pounds equivalent of TNT (trinitrotoluene), whereas nuclear detonations result in blast wave equivalent to thousands or millions of tons of conventional explosives. Rapid expansion of gases from explosive resulting in rapid compression of surrounding air creates shockwaves which travel in all directions at supersonic speeds.

Blast overpressure is the abnormal increased pressure, its magnitude depends on energy released on detonation, distance from the point of detonation, time elapsed since explosion and measurement technique. Blast front is the leading edge of the wave that interrupts undisturbed air. At the point of explosion, rapidly expanding gases create a pressurized zone at the blast front but as the gases keep moving, a negative pressure zone is left behind the blast front which also moves away from detonation spot. Negative pressure zone moves at a slower speed as propagation speed depends on the density of the air thus the pressure in the region, and is believed not to contribute to blast injury.

TBI due to explosions or blasts is divided into four type's primary, secondary, tertiary and quaternary blast injury. Brains response to the initial blast wave causes primary injury due to the transmission of pressure wave through brain tissue. Projectiles

of mass (shrapnel) penetrating the head causes secondary injury. Acceleration forces on the head due to the movement of the body caused by blast wind s result in tertiary injury. Hemorrhagic shock and chemical or thermal burns which are not caused by the previous three types of injury comes under quaternary injury.

The most critical and most intriguing part of these four injuries is the primary injury. Transmission and reflection of blast wave through the brain, its effects on biological function of the brain and cause of damage ranging from body level to tissue and further to cellular level is a debated to date. Primary blast wave contains two parts, shockwaves and blast wind or supersonic air movement.

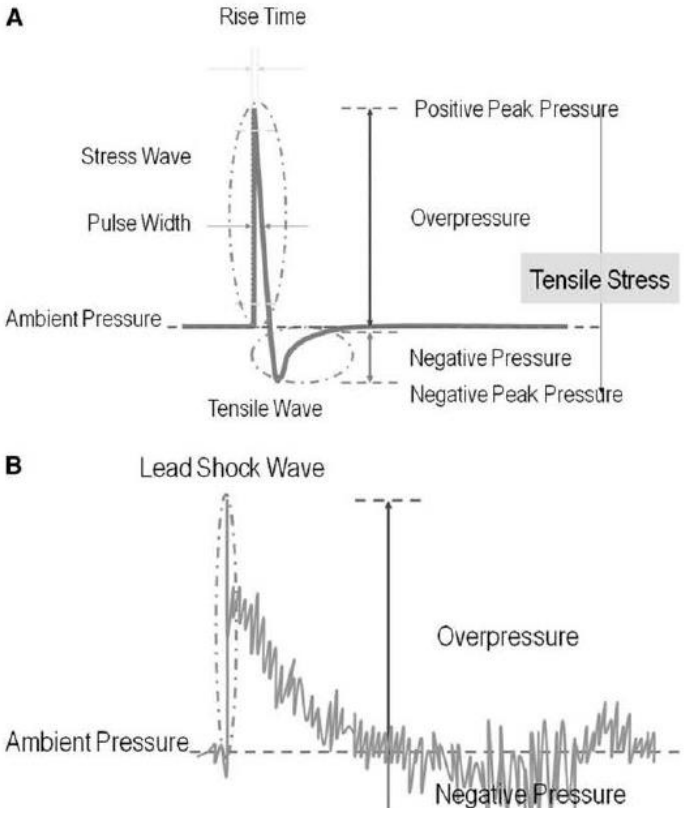

Figure 2-8 Pressure profile of (a) Shockwave and (b) free-field blast wave modeled by Friedlander wave form[12]

Shockwaves are nonlinear, discontinuous, infinite amplitude acoustic pressure wave pulse and occur over a time range of around a microsecond. During this short duration pressure increases rapidly to 100MPa and then decreases to a pressure lower than atmospheric pressure. Pressure profiles of Shock wave and blast wave seems similar as they have positive pressure components followed by brief negative components as shown in figure 2-8 (a) and (b) (Nakagawa, et al., 2011). Extremes of these pressure values, rise time, pulse width altogether determines the damage caused during this exposure. Compression, shearing and tensile stress are the direct effects of Shockwaves on tissues, whereas indirect effects relate to shock /bubble interaction (Nakagawa, et al., 2011). Rise time is the duration over which pressure increases from 10 % to 90 % of the maximum positive value. Pulse width is the duration over which pressure remains over certain level typically half of extreme positive value.

2.6 Health Effects

The characteristic symptom of TBI is disturbed cognition which challenges memory, attention, learning and coordination. TBI also affects behavior, emotion and motor function. Headaches, fatigue and sleep disorders are other significant signs. Secondary neurologic disorders typically mood disorders, post traumatic epilepsy may occur following TBI which may disturb life. One general classification of TBI is based on the patient's symptoms. Symptoms vary from case to case and some of these can be mitigated on diagnosis whereas rest persist and lead to a disability.

TBI is classified using Glasgow Coma Scale for clinical purposes. Originally drafted by Teasdale and Jennett in 1974 to assess unconsciousness or coma, it was adopted to assess TBI (Teasdale & Bryan, 1974). It is a neurologic scale depending on

three factors eye opening, verbal response and motor response. All three scores are added to give a final score which helps in assessing unconsciousness.

Table 2-1 Glasgow Coma Scale [6]

Ability	**Score**
Eye opening (E)	
Spontaneous	4
To voice	3
To pain	2
None	1
Motor Response (M)	
Normal	6
Localized to pain	5
Withdraws to pain	4
Abnormal flexion to pain	3
Abnormal extension to pain	2
None	1
Verbal Response (V)	
Normal Conversation	5
Disoriented Conversation	4
words, but not coherent	3
No words, only sounds	2
None	1
Score(E)+(M)+(V)	3 to 15

But since unconsciousness can be associated with other factors like other organ failure, medical influence and intoxications due to alcohol or drugs, GCS alone cannot be used to assess TBI. Other procedures such as computed tomography (CT) scans, duration of post –traumatic amnesia, loss of consciousness, Abbreviated Injury scale used together help in assessing the injury severity (Frieden, Houry, & Baldwin, 2014).

Table 2-2 Abbreviated Injury Scale [6]

Criteria	***TBI Severity***		
	Mild	***Moderate***	***Severe***
Structural Imaging	Normal	Normal or abnormal	Normal or abnormal
Loss of consciousness	<30 minutes	30 minutes to 24 hours	>24 hours
Post traumatic amnesia	0-1 day	>1 and <7 days	>7 days
Glasgow Coma Scale score	13-15	9-12	3-8
Abbreviated Injured Scale Score:Head	1-2	3	4-6

2.7 Cellular level Damage mechnaism

As discussed earlier, loads at macroscale are transferred to cellular level in the form of axonal stretch, shown in figure 2-7. The strain rate effect leading to the damage of axons is due to the viscoelastic behavior. This can be best explained by considering Silly Putty, which can be molded into a cylindrical shape, which when pulled slowly will elongate considerably. But the same material when pulled rapidly breaks into two. This is

the same mechanism involved in the injury to axonal cytoskeleton (Smith & Meaney, 2000).

Primary axotomy is the immediate breakage of axons upon application of rapid stretch, but this is a rare phenomenon except during severe brain injury. Intracranial dural compartments also play an active role in addition to the loads applied in determining the amount of damage experienced. During rotation of head in coronal plane, falx membrane separating the two hemispheres of brain resists the motion of trailing brain hemisphere, while the leading hemisphere pulls away. This results in a high strain along sagittal midline which is translated to stretch forces on axons passing through splenium of the corpus callosum.

2.7.1 Axonal Pathology

Normally axons are ductile in behavior and they return to their original length upon removal of loads. But, when the loads are applied rapidly they exhibit a brittle behavior. It was observed that within seconds of injury, axons are undulated temporarily, misaligned and lose elasticity (Tang-Schomer, Patel, Baas, & Smith, 2010). Even though the axons return to prestretch orientation, it is followed up with the appearance of periodic swellings along length of axon within few hours as shown in figure 2-9 (Smith & Meaney, 2000). These swellings are known as “Axonal varicosities”. The mostly seen symptom following injury is the "Axonal bulb" (also called "retraction ball" earlier) .Axonal bulb is the single large swelling at the end of the axon or axon connections and it indicates complete disconnection. Axonal bulb formation and following axonal degeneration is shown in figure 2-10 (Smith & Meaney, 2000).

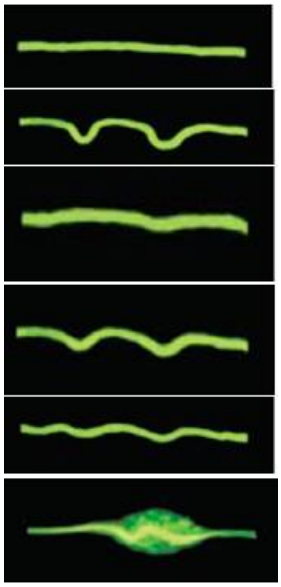

Figure 2-9 Undulations following Dynamic stretch injury and Delayed elasticity of axon [16]

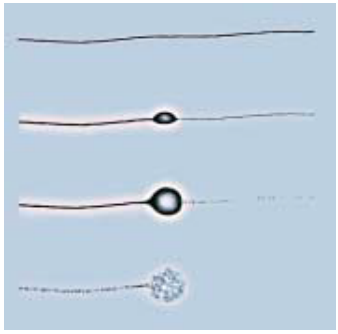

Figure 2-10 Illustration of axonal bulb formation showing axon disconnection [16]

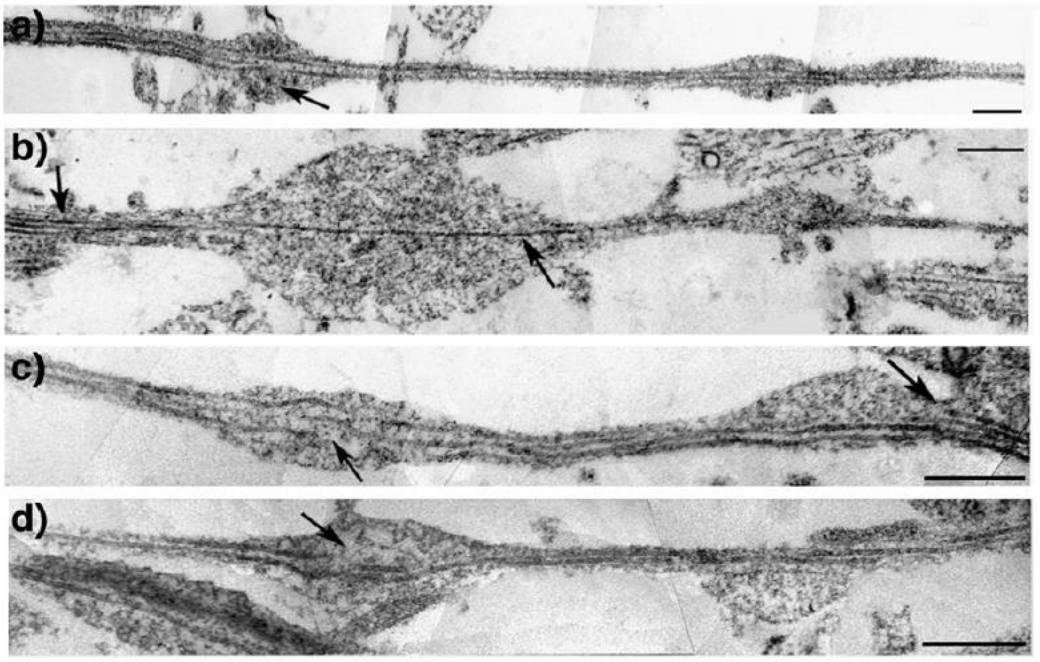

Figure 2-11 (a), (c), (d) Broken MTs at varicose swellings. (b) Intact single MT traversing a axonal swelling [20].

Tang-Schomer et al., have studied the process of delayed elasticity observed in axon recovery. They have attributed this to the microtubule failure mechanism. When observed using Transmission electron microscope (TEM), peaks of the undulated axons contained significantly altered microtubule configurations. Peaks of these undulations were found to contain broken microtubules as shown in figure 2-11 (Tang-Schomer, Johnson, Baas, Stewart, & Smith, 2012). The free ends of these microtubules appeared to be as if undergoing catastrophic depolymerization. This twisting and breaking of microtubules doesn't allow axon to return to prestretch orientation. But subsequently after the breakage microtubules depolymerize, allowing the axon to be free of undulations. This comes at a cost of axonal transport interruption. This whole mechanism of axonal transport interruption is summarised in figure 2-12 (Tang-Schomer, Johnson, Baas, Stewart, & Smith, 2012).

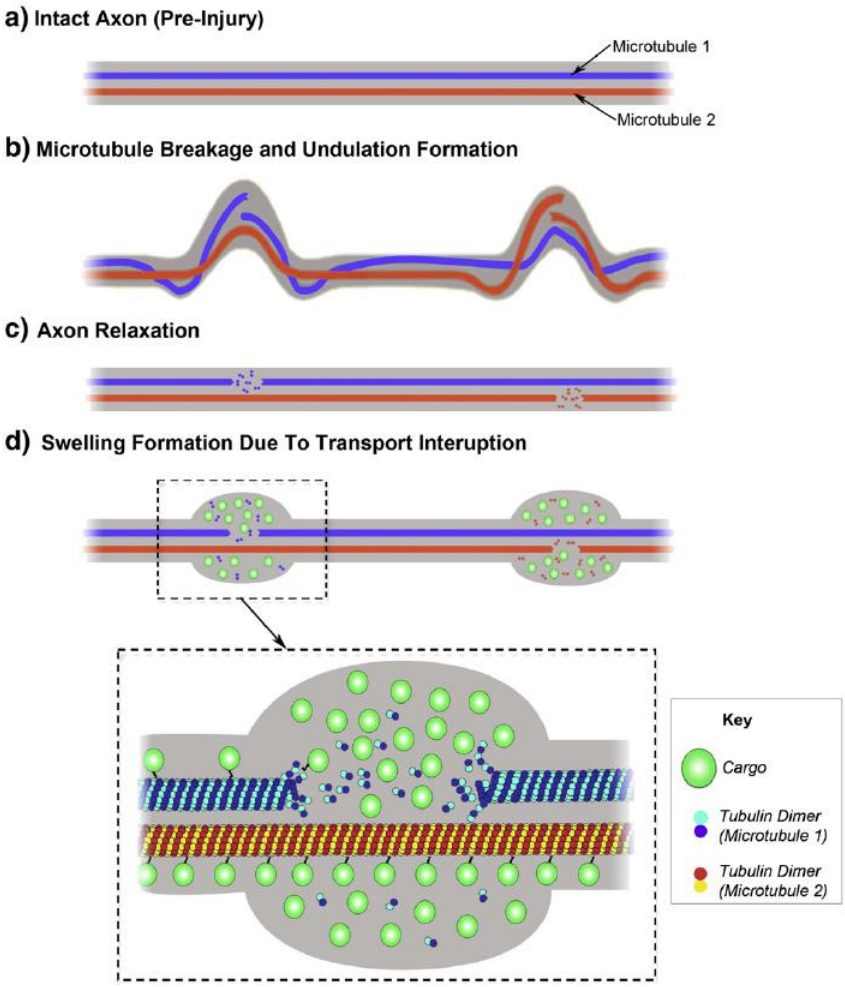

Figure 2-12 Mechanism of axonal swelling [20]

2.8 Mechanics of Brain Deformation

Holbourn (1943) has discussed the properties of the brain and the mechanics involved in the failure. According to him, Density of brain tissue, cerebro spinal fluid, blood is almost the same as water and compressibility of brain under hydrostatic pressure is less and is comparable to water. It might take 10000 tons to shrink brain to

half its volume (Holbourn, 1943). Rigidity of the brain is very less and it deforms a lot under slightest of pressures, in quite contrast to skull which requires 1 ton of load to reduce the diameter by 1cm.

From these points he proposed that in materials like brain, whose bulk modulus is far greater than modulus of rigidity, the modes of failure are by shear strain. Irrespective of skull fracture, shear stains are experienced in the brain, the only difference would be the point of skull fracture would show superficial signs of damage in the immediate neighborhood. He proposed that linear acceleration forces tend to produce compression strains which may not be injurious due to the high bulk modulus as explained earlier. For blows lasting long, injury is not dependent on the time for which force acts. For shorter duration blows injury is proportional to the force multiplied with its duration

2.9 Mechanical Properties of Brain Tissue

Creep properties of the brain were studied by Dodgson in 1960. Later a lot more of these tests were conducted to the current day. Methodological errors have resulted in large variation in the results reported. The common causes of these errors were

a.) Use of dead tissues or delayed use of tissues for testing, leading to property changes.

b.) Extraction of linear viscoelastic part from results of large deformation In vitro Behavior

Linear viscoelastic regime characterization is usually used in complex materials to determine properties such as shear modulus or elastic modulus independent of applied

strain magnitude. Linear viscoelastic limit is determined using slower increments in strains and observing the onset of change of material functions. From the data obtained below linear viscoelastic limit, material functions such as relaxation modulus G(t), Creep modulus J(t), storage modulus G'(ω) and loss modulus G''(ω) can be derived. Behavior at larger strains is estimated using these functions. According to studies by Bliston and Nicolle, Linear viscoelastic strain limit of brain tissue is very small, around 0.1 to 0.3% (Bliston, Liu, & Phan-Thien, 1997), (Nicolle, Lounis, willinger, & Palierne, 2004), and many studies which have ignore this lead to errors in the results published.

2.10 Strain and Strain rate Dependence

Mechanical deformation of axons or strain is thought to be the key factor in damage caused during traumatic axonal injury. It was thought that mechanical deformation results in neurofilament structure damage in axonal cytoskeleton. Threshold limits for deformation has been studied earlier for in vivo axons of CNS using squid giant axon (Galbraith et al., 1993), frog sciatic nerve (Gray and Ritchie,1954), rat tibial nerve(Ry-devik et al., 1990) and pedal nerve of the slug (Jenkins and Carlson, 1904). These results were supplemented with physical and computational models which together helped in setting up tolerance limits. Smith et al have examined dynamic deformation of axons in vitro and published the threshold for primary axotomy. 26 to 35 sec^{-1} is the range of strain rates typically seen in a traumatic brain injury (Smith, wolf, Lusardi, Lee, & Meaney, 1999).

2.11 Viscoelasticity

2.11.1 Relaxation and Creep tests

To characterize the viscoelastic behavior of a material the basic method used are the relaxation test and the creep test. In relaxation test a specimen is considered to be at particular strain, starting from beginning of time and all through the duration of the test. It

is very important that there is no stress history in the specimen and if present it needs to be removed using some methods like annealing. After some time due to the memory of the material, stress required to maintain the strain in the specimen is reduced with time reaching zero for an ideal thermoplastic polymer or remains a constant value for thermoset polymer. Due to the stress varying with time and strain being constant modulus varies with time, it can be written as

$$E(t) = \frac{\sigma(t)}{\varepsilon_0}$$

Where E(t) is called the relaxation modulus. Moduli values at initial and infinite times in a thermoset are defined as Initial modulus and Equilibrium modulus respectively.

In a Creep test the specimen is loaded with constant stress at the beginning of time and the same care is taken as in relaxation test to avoid having any stress history. Here strain increases with time under constant stress and as earlier the relationship can be written as

$$D(t) = \frac{\varepsilon(t)}{\sigma_0}$$

Where D(t) is called the creep compliance. Linearity and non-linearity of the material can also be established from these tests by conducting these tests at various times and observing the results. Other loading methods such as constant strain rate and steady state oscillation can also be used.

2.11.2 Mechanical models

Viscoelastic models can be formed by various combinations of spring and damper which are named differently and behave in different manners. They are Maxwell Fluid model, Kelvin Solid model, three parameter solid model and four parameter fluid model. These are shown in the figure 2-13

Maxwell model behaves like a fluid due to the free damper providing unlimited strain for a finite stress application. Kelvin model behaves like a solid due to the free spring providing limited deformation for a given force. Maxwell or any model with free damper acts like a thermoplastic whereas any model with free spring acts like thermoset. Here emphasis is onto kelvin model of viscoelastic behavior as the work done used this.

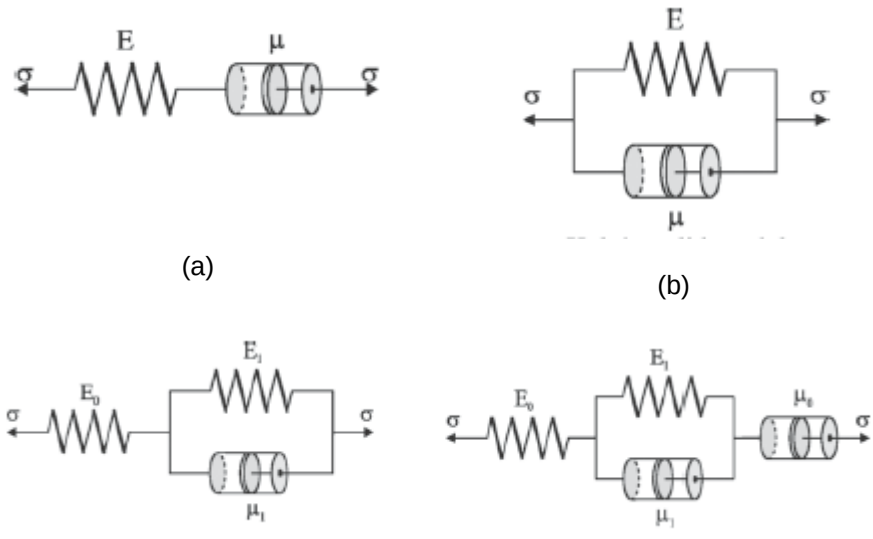

Figure 2-13 Viscoelastic models (a) Maxwell model (b) Kelvin model (c) Three parameter solid model (d) Four parameter fluid model

Chapter 3

Modified Shear Lag model

As discussed earlier, we have assumed a two parameter Kelvin viscoelastic model for approximating the properties of microtubules and tau proteins.

3.1 Stress strain relationship for a Kelvin solid model.

For the Kelvin solid model shown in figure 2-13 (b), Equilibrium equation for the entire model can be written as

$$\sigma = \sigma_s + \sigma_d \tag{3.1}$$

Kinematic condition is

$$\varepsilon = \varepsilon_s + \varepsilon_d \tag{3.2}$$

Constitutive equations or stress strain relationships are

$$\sigma_s = E\varepsilon_s \tag{3.3}$$

$$\sigma_d = \mu\dot{\varepsilon}_d \tag{3.4}$$

By combining equations (3-1) to (3-5) we get

$$\sigma = E\varepsilon_s + \mu\dot{\varepsilon}_d \tag{3.5}$$

3.2 Model and governing equations

As discussed in detail in Hossein et al , Brady et al, axon structure consists of neurofilaments, microtubules (MTs) crosslinked with tau proteins and other organic components (Ahmadzadeh, Smith, & Shenoy, 2014), (Brady, Siegel, Albers, & Price, 2005). MTs function both as organelle transport tracks and also structural elements. It was found in the recent studies that damage to MTs has led to greater reduction in axon strength compared to other axon structures such as neurofilaments (Ouyang, Nauman, & shi, 2010). Hence we have adopted a hexagonal microtubule lattice cross linked by tau proteins as shown in figure 3-1. Following the electron micrograph studies previously

conducted, we assume a staggered distribution of MTs, with alternate rows of MTs staggered with respect to their neighbors by a distance L as shown in figure 3-1. A hollow cylindrical section with outer radius R_O and inner Radius R_I is assumed for MT. Individual MTs are surrounded by neighboring MTs and the α-value of six results in a hexagonal distribution as assumed earlier. MTs spacing (distance between neighboring MTs) is denoted by d_M and distance between neighboring tau proteins is denoted by d_T.

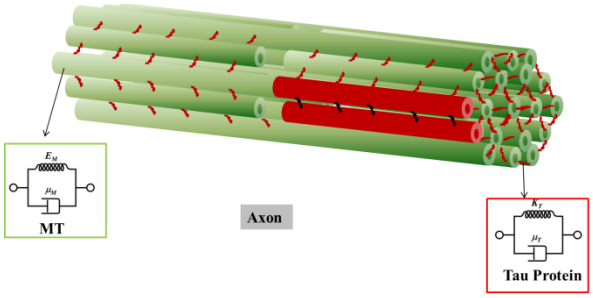

Figure 3-1 Axon microstructure consisting of MTs crosslinked by tau proteins

In the study by Ahmadzadeh et al, Tau proteins were assumed to be viscoelastic and they were approximated using a two parameter viscoelastic model (Ahmadzadeh, Smith, & Shenoy, 2014). But as recent studies provide evidence of viscoelastic behavior in MTs (Lin, Koenderink, Mackintosh, & Weithz, 2007) we have approximated MTs using the two parameter viscoelastic model as well, as shown in Figure 3-1.

The spring stiffness and viscosity of tau protein are denoted by K_T and μ_T respectively. These values are obtained from AFM experiments conducted in previous studies and used by Ahmadzadeh et al (Wegmann, Scholer, Bippes, Mandelkow, & Muller, 2011). Youngs modulus and viscosity of MTs are represented by E_M and μ_M respectively. These values are obtained from MD simulations and reported by Adnan et al (Adnan, Qidwai, & Bagchi). To obtain dynamic response of axon at different strain rates we derive and solve rate depending viscoelastic shear lag model. The unit cell used here is shown below in figure 3-2.

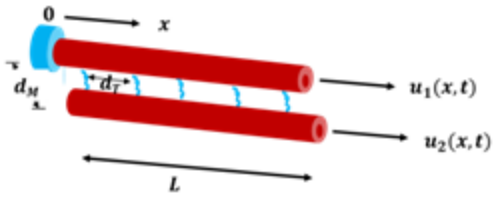

Figure 3-2 Unit cell

The force-displacement relation for viscoelastic tau protein is described as

$$\eta\dot{\delta} + \delta = \frac{F}{K_T} \tag{3.6}$$

Where the dot represents the time derivative, and

$$\eta = \frac{\mu_T}{K} \tag{3.7}$$

Similarly viscoelastic stress-strain relation for MT is described as

$$E_M\varepsilon_M + \mu_M\dot{\varepsilon}_M = \sigma_M \tag{3.8}$$

As axons are loaded, tau proteins rate dependent deformation aids the force transfer from MT to the neighboring MTs. The shear stress developed on the surface of the MT due to tau protein deformation is illustrated in figure. Here we placed a Cartesian coordinate system such that origin lies at center of the MT and x axis lies in the axial direction of MT. A unit cell comprising two staggered MTs is used and longitudinal displacement fields for these two MTs are defined by *u1(x,t)* and *u2(x,t)* respectively. Thus tau protein elongation is given by

$$\delta_T = u_2(x,t) - u_1(x,t) \tag{3.9}$$

To convert force in tau protein to shear stress on MTs

$$\tau = \frac{f}{A} \tag{3.10}$$

Where *A i*s the projected area and *f* is the component of force in the longitudinal direction given by

$$f = F * \cos(\beta) \tag{3.11}$$

$$A = 2(R_O - R_I) * d_T \tag{3.12}$$

Where β is the angle between tau protein and the MT assumed here as 60^o.

Using force balance in the axial direction from the free body diagram as shown in figure 3-3, we converted shear stress can be converted into normal or axial stress.

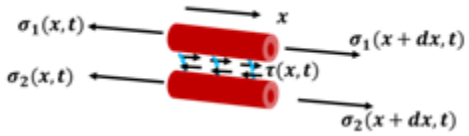

Figure 3-3 Free body diagram

$$\sigma_M^1 \pi\left({R_O}^2 - {R_I}^2\right) + \partial\sigma_M^1 \pi\left({R_O}^2 - {R_I}^2\right) - \sigma_M^1 \pi\left({R_O}^2 - {R_I}^2\right) = 2\alpha\tau * \partial x * (R_O - R_I) \tag{3.13}$$

$$\Longrightarrow \frac{\partial\sigma_M^1}{\partial x} = \frac{2\tau\alpha}{\pi(R_O + R_I)} \tag{3.14}$$

Similarly from the force balance of the second microtubule we get

$$\frac{\partial\sigma_M^1(x,t)}{\partial x} = -\frac{\partial\sigma_M^2(x,t)}{\partial x} = -\frac{2\alpha}{\pi(R_O + R_I)}\tau(x,t) \tag{3.15}$$

Where the superscripts 1 and 2 denote MT1 and MT2 respectively

$$\varepsilon_M = \dot{\varepsilon_M} t \tag{3.16}$$

From stress strain relationship used earlier,

$$\sigma_M = \left(E_M + \frac{\mu_M}{t}\right)\varepsilon_M \tag{3.17}$$

$$\Longrightarrow \sigma_M = \left(E_M + \frac{\mu_M}{t}\right)\frac{\partial u(x,t)}{\partial x} \tag{3.18}$$

$$\Longrightarrow \frac{\partial\sigma_M}{\partial x} = \left(E_M + \frac{\mu_M}{t}\right)\frac{\partial^2 u(x,t)}{\partial x^2} \tag{3.19}$$

Combining these above equations, we obtain a system of partial differential equations as

$$-2L_c^2(x,t)\frac{\partial^2 u_1(x,t)}{\partial x} = 2L_c^2(x,t)\frac{\partial^2 u_2(x,t)}{\partial x} = \eta\big(v_2(x,t) - v_1(x,t)\big) + u_2(x,t) - u_1(x,t) \quad (3.20)$$

Where $v_i(x,t) = \dot{u}_i(x,t), i = 1,2$, and

$$L_c = \left[\frac{\pi(R_O^2 - R_I^2)d_T\left(E_M + \frac{\mu_M}{t}\right)}{2\alpha K_T cos(\beta)}\right]^{\frac{1}{2}} \quad (3.21)$$

Here Lc is the length over which transfer of stresses in microtubules occur.

To obtain the non-dimensional form, spatial and temporal coordinates are rescaled using the equations $X = x/L$ and $T = \dot{\varepsilon}t$. Similarly displacement and velocity fields are rescaled as $U_i(x,t) = u_i(x,t)/L$ and $V_i(x,t) = \dot{u}_i(x,t),/L\dot{\varepsilon}$, respectively $(i = 1,2)$. Equation can be rewritten as

$$-2\frac{L_c^2}{L^2}\frac{\partial^2 U_1(X,T)}{\partial X^2} = 2\frac{L_c^2}{L^2}\frac{\partial^2 U_2(X,T)}{\partial X^2} = \eta\dot{\varepsilon}\big(V_2(X,T) - V_1(X,T)\big) + U_2(X,T) - U_1(X,T) \quad (3.22)$$

Displacement of one end of unit cell is specified as a function of strain rate while holding the other end fixed to obtain the mechanical response. Force free boundary conditions are also applied as shown below.

$$U_1(0,T) = 0 \quad (3.23)$$

$$U_2(1,T) = T \quad (3.24)$$

$$\frac{\partial U_1(1,T)}{\partial X} = \frac{\partial U_2(0,T)}{\partial X} = 0 \quad (3.25)$$

3.3 Variation of Parameters

Scaled governing equations imply that model response depends on two dimensionless parameters, L/L_c and $\eta\dot{\varepsilon}$, which stand for scaled half-length of MTs and scaled rate of loading respectively. Both these parameters depend on axon's geometric

and material parameters. These material and geometric parameters are applied based on the previous studies and are detailed in Table 3-1.

Table 3-1 Values used for material and geometric parameters

Parameter	Quantity	Value	Ref.
R_O	MT outer radius	12.5nm	2
R_I	MT inner radius	7nm	2
E_M	MT Young's modulus	2GPa	2
d_T	Tau protein spacing	30nm	2
2L	MT length	Short: 2µm Long: 10 µm	2
K_T	Tau protein spring constant	0.25pN/nm	2
η	Tau protein dashpot timescale	0.35s	2
µM	MT viscosity	70Pa.s	1

Here to observe the onset of MT failure and axon breaking (axotomy), we need to have an idea of what strain it takes to break MT's. Janmey et al. reported that strains in excess of 50% lead to failure of MT network under shear deformation (Janmey, Euteneuer, Tarub, & Schliwa, 1991). Based on this and Hossein et al, we have considered critical strain for MT failure to be 50%.

Dynamic stretch experiments show that, axons can be stretched up to twice their length (in other words, 100% strain) without any MT damage under quasi static loading

($0.01s^{-1}$). But when subjected to dynamic loading, i.e. strain rates in the range of 22-44 s^{-1} and strains exceeding 65% MT failure was observed (Ahmadzadeh, Smith, & Shenoy, 2014). With these strain rate values, we obtained $\eta\dot{\varepsilon}$ values in the range of 0.001 to 15, corresponding to quasi static and dynamic loading rates respectively.

Using α value of 6 for the hexagonal lattice, tau protein spacing d_T of 30nm and β value of 60^o for the angle between tau protein and MTs we obtained a Lc value of 3.57 using eqn (3-21).We have chosen the length of short MTs to be 2μm and long MTs to be 10μm which gives us L/L_c ratios of 0.28 and 1.40 respectively. Using these L/Lc values, strain rates were varied to study the mechanical response of the axon.

We have employed Mathematica to solve the governing equations (3-22) analytically and obtained the numerical solutions using the data obtained.

Chapter 4

Results and Discussion

The deformation criteria of this model are sliding of MTs facilitated by the elongation of tau proteins or MT stretching leading to microtubule breaking. Axons mechanical response depends only on two dimensionless parameters L/Lc (scaled half length) and $\eta\dot{\varepsilon}$ (scaled rate of loading) based on equation (3-22).

As discussed earlier, we have varied the strain rates to go from quasi static loading to dynamic loading. Quasi static loading strain rates ranged from $0.01s^{-1}$ to $1s^{-1}$. Dynamic loading range was chosen from 22 – $44s^{-1}$ (Ahmadzadeh, Smith, & Shenoy, 2014). We have applied a strain of 10%.

4.1 Effect of Strain rate on Tau Protein Elongation

Tau proteins elongation strongly depends on strain rate due to their viscoelastic properties. The stiffness of tau proteins depends on rate of stretch. If pulled at higher strain rates the polymer bonds become stiff whereas at lower strain rates, the polymer chains uncouple easily allowing tau protein to stretch in length. Load transfer mechanism from one MT to other differs because of this. We have plotted the result of tau protein elongation for short (L=1μm)and long MTs (L=5 μm) due to strain rate in figure 4-1 and figure 4-2.

We found that tau protein elongation varies with strain rate as discussed earlier. It also varied with the position of tau proteins along the length of microtubules. Overall length also played a major role in tau protein elongation. Based on these three factors it can be seen in figures 4-1 and 4-2tau protein is elongation is significant at lower strain rates ($\eta\dot{\varepsilon}$ =0.001), in both short and longer MTs. But at higher strain rates, tau protein elongation is insignificant in longer MTs whereas it's less in short MTs. It can also be

seen that the tau protein elongation is not uniform along the length of MTs which is a feature of shear lag models.

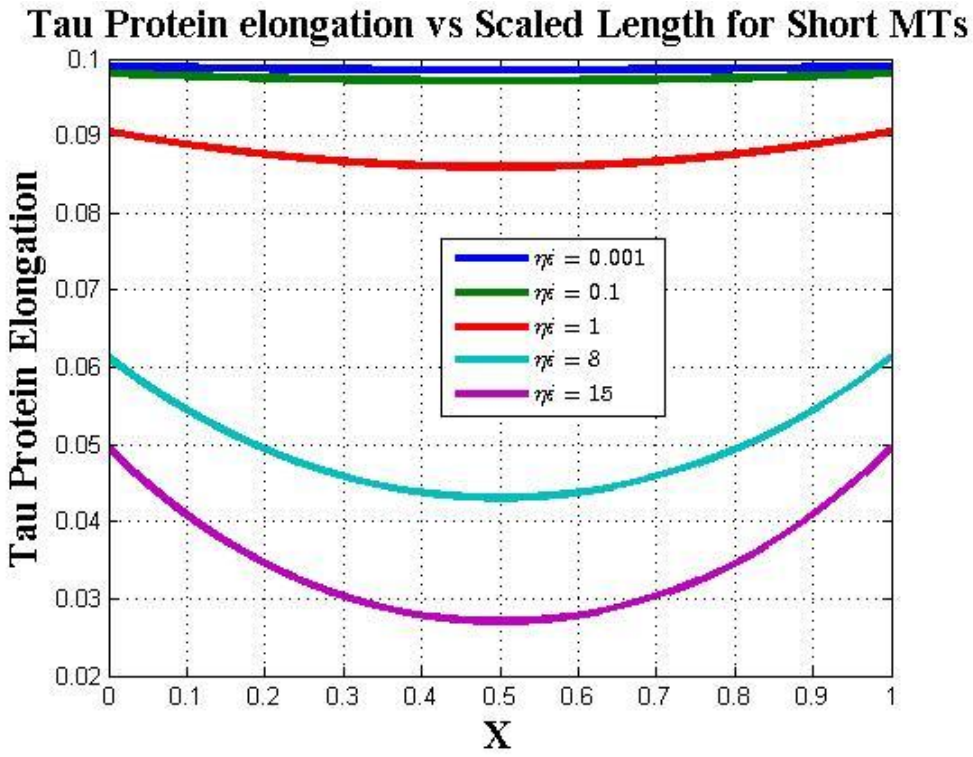

Figure 4-1 Tau Protein Elongation vs scaled half length for L=1μm

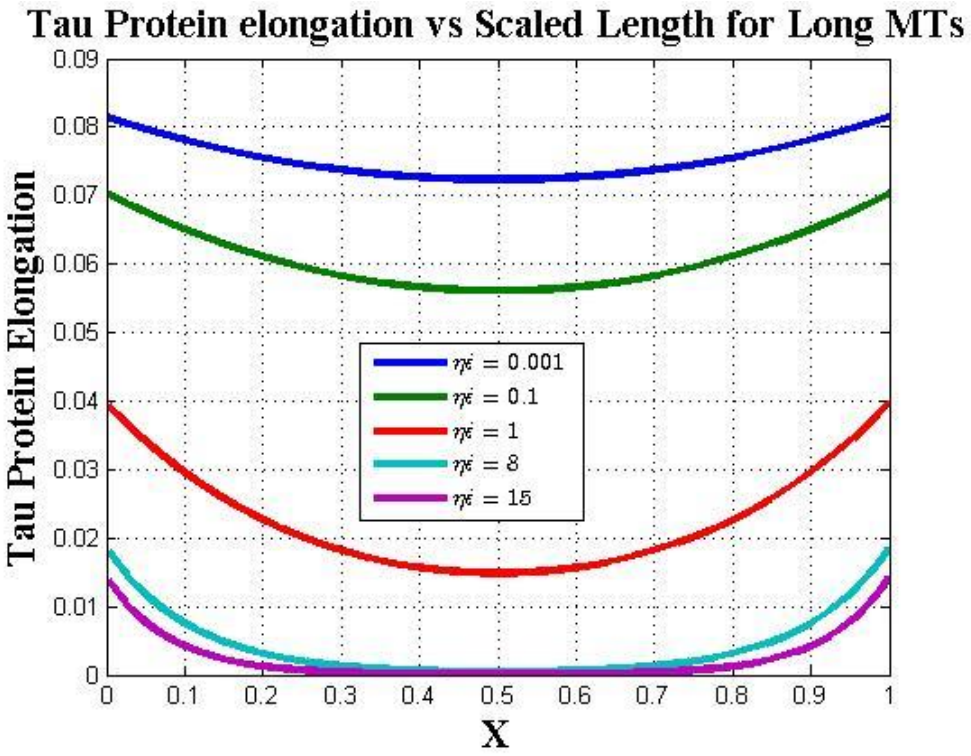

Figure 4-2 Tau Protein Elongation vs scaled half length for L=5μm

4.2 Effects of Strain rate on MT elongation

Variation of tau protein elongation with strain rates leads to variation in MT elongation, as tau proteins tightly bind the microtubules. We have applied a strain of T=0.1 on the second MT at X=1 (X=L/Lc) and found the axial strain developed in MT1. These strains with varying loading rates are plotted against scaled half-length as shown in figures 4-3 and 4-4 for short and long MTs respectively. It can be seen that for short length, MT1 does not elongate significantly at quasi static strain rates. This can be associated with the significant tau protein elongation thus facilitating MT sliding rather than stretching. Whereas at higher strain rates, MT1 showed significant elongation as can be seen in figure 4-3 due to viscoelastic nature of tau proteins, resulting in stiff

behavior. Stiffer tau proteins cause MT1 to stretch and at higher strains may lead to breaking of MTs.

In the case of longer MTs also the strain in MT2 under same loading conditions , MT1 shows significant elongation in the sense almost 2 times the elongation observed in the case of short MTs. Overall behavior is the same, less MT stretch at lower strain rates and greater stretch at higher strain rates. It is also observed that microtubules experience greater strain at the center and there is almost no stretch at the free ends. This is one of the reasons for longer MTs to break at the center leading to failure.

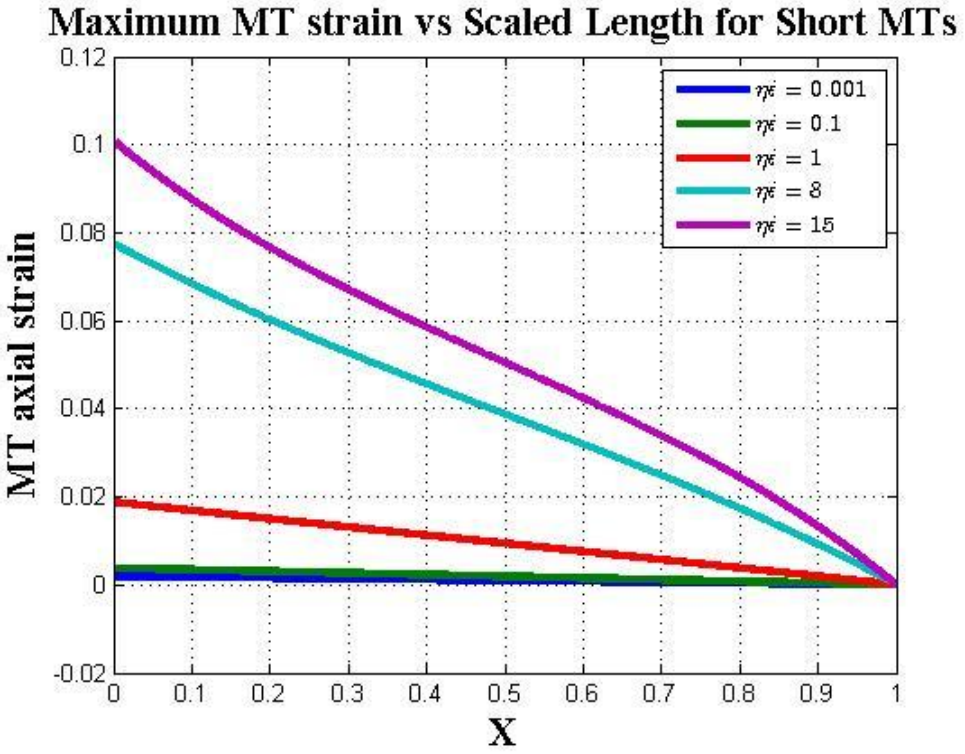

Figure 4-3 MT strain vs scaled half length for L = 1μm

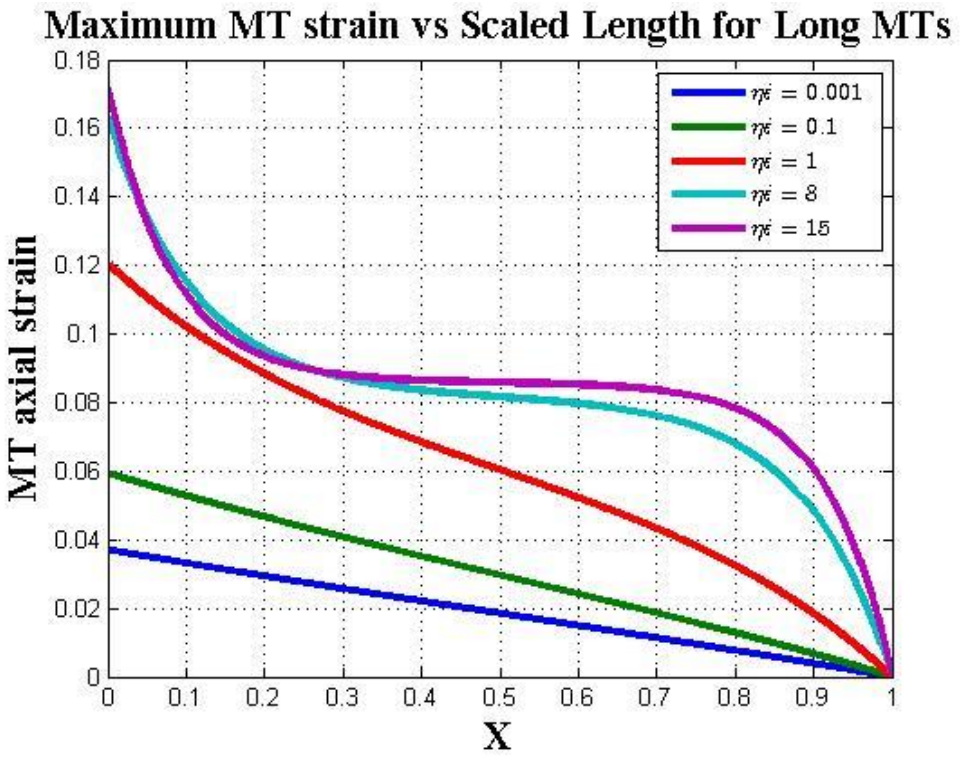

Figure 4-4 MT strain vs scaled half length for L = 5μm

4.3 Effect of $\eta\dot{\varepsilon}$ and L/L_C on axon failure

Differences in applied axonal strains leads to difference in the MT strains observed which is normal. We have tried to see this behavior coupled with the strain rate effect as can be seen from the plots in figures 4-5 to 4-8. As it can be seen in figure 4-5, the short length MTs with half-length of 1μm doesn't reach assumed strain limit of 50% even at dynamic loading rates, whereas from figure 4-6, long MTs with half-length of 5μm fails at dynamic loading rate.

We have also checked variation of tau protein spacing on characteristic length. As can be seen from equation 3.21 it is observed that as tau protein spacing increases characteristic length also increases. Thus it can be expected that the strains experienced

in the MTs are less compared to the normal case. We have doubled the tau protein spacing from 30nm to 60nm and the model response for strain was plotted in figures 4-7 and 4-8 respectively. It can be observed that strains experienced in MTs are slightly lower for the corresponding strain rates, when the tau protein spacing was increased.

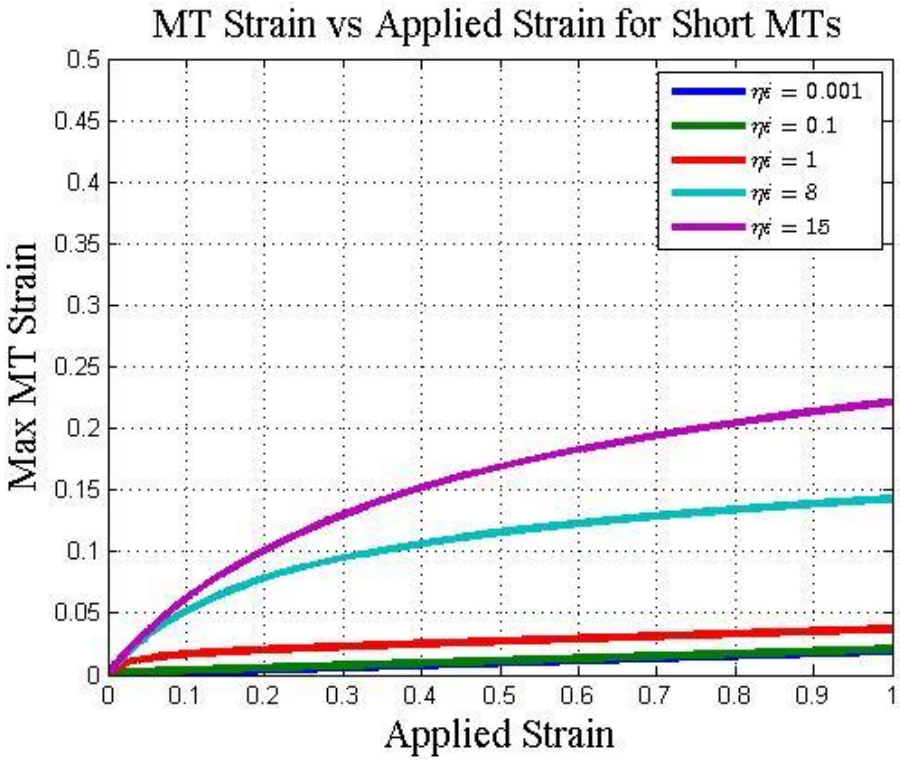

Figure 4-5 MT strain vs Applied strain for L/Lc = 0.28

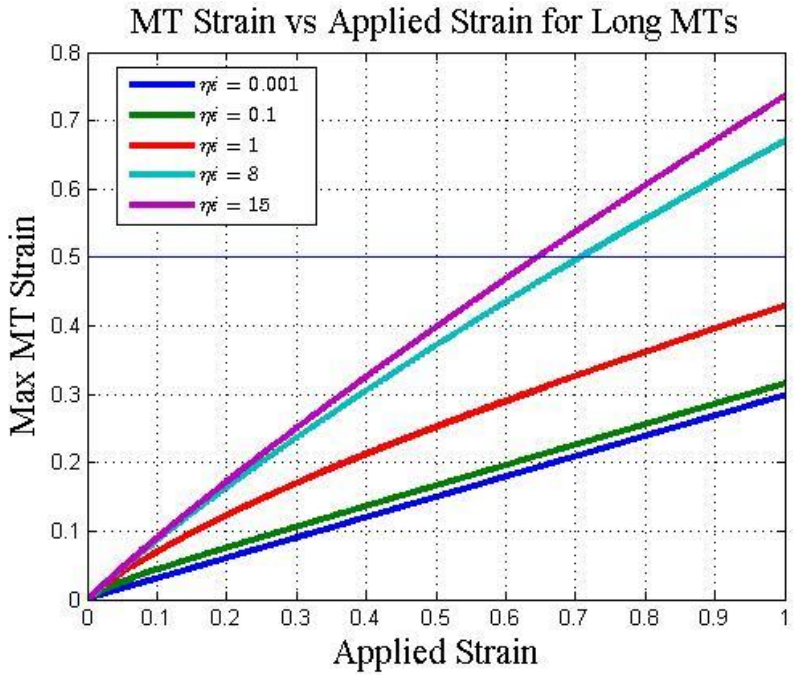

Figure 4-6 MT strain vs Applied strain for L/Lc=1.40

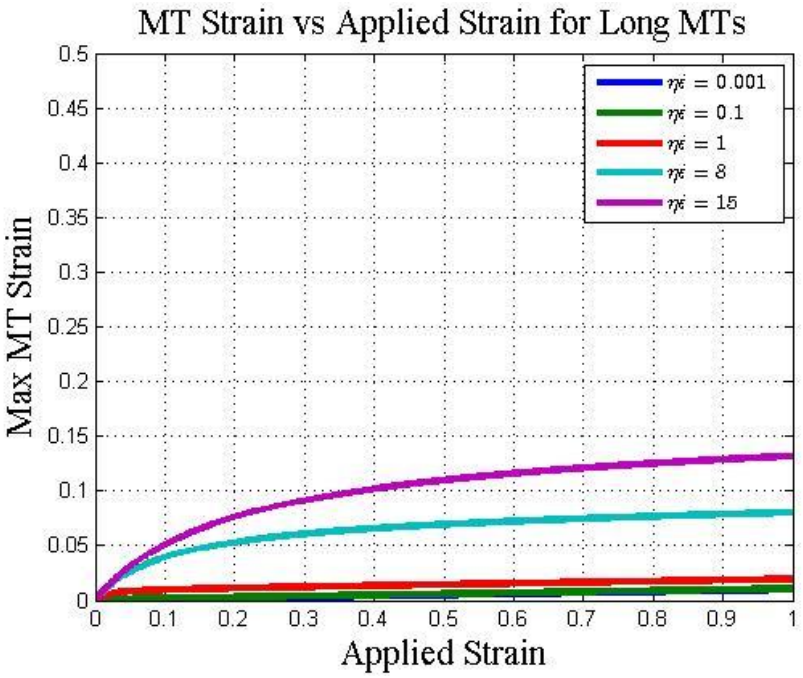

Figure 4-7 MT strain vs Applied strain for L/Lc=0.20

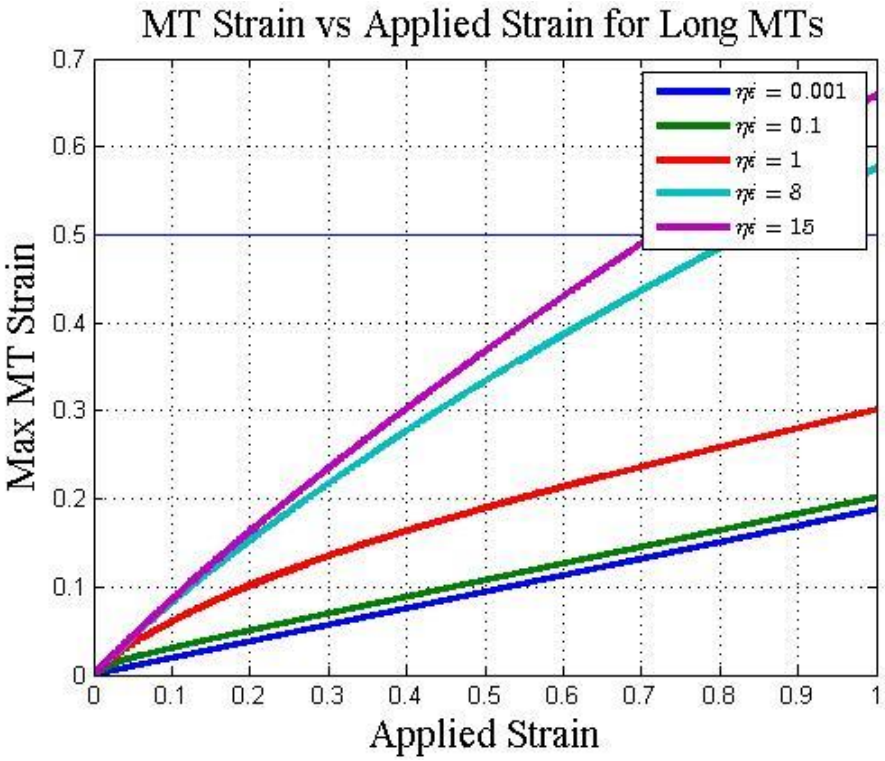

Figure 4-8 MT strain vs Applied strain for L/Lc=1.00

Chapter 5

Conclusion

We have implemented a modified viscoelastic shear lag model to determine mechanical response of axon under different strain rate loading conditions. We have modeled the axon structure to contain microtubules crosslinked by tau proteins. We have modeled both tau proteins and microtubules behavior to be viscoelastic using two parameter Kelvin model. We have studied the damage criteria at fast and slow loading rates, corresponding to axonal stretch injury.

Our analysis suggests that when axons are loaded with tensile strains, they can be deformed either by large scale MT elongation or tau protein elongation. Large scale elongation of microtubules is catastrophic as MTs have a failure strain limit of 50%. Tau proteins are biopolymers which can accommodate large stretch without failure. Large scale elongation of tau proteins leads to reversible sliding of microtubules. But these biopolymers are viscoelastic, which makes them stiffer at higher strain rates, resulting in MT elongation.

Based on this analysis we can conclude that dynamic mechanical loading of axons can result in MT failure or reversible tau protein stretching. Using the data from MT strain graphs plotted earlier in addition to data obtained from higher strain ranges up to 300% we have obtained a phase diagram between strain and strain rates varying the length of MTs, as shown in figure 5-1 It illustrates the regions where the axons fail due to applied strain for a particular rate of loading based on their length. As shown in figure 5-1 regions to the left of the curves (each curve for a particular length of MTs), experience reversible sliding of MTs , whereas regions to right of the curve experience MT stretch causing failure of axonal cytoskeleton.

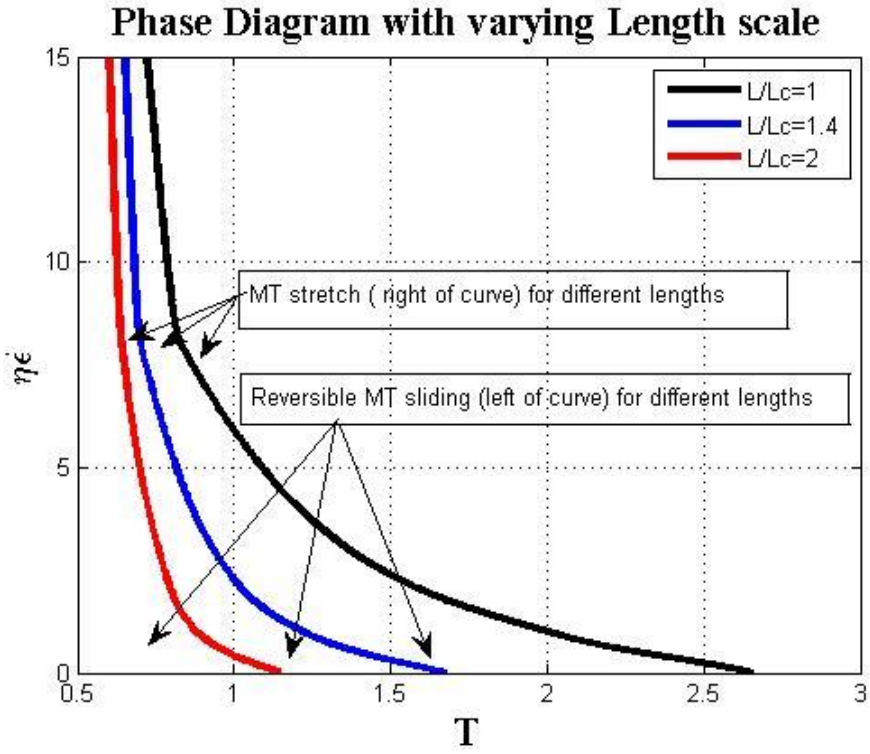

Figure 5-1 Phase diagram demarcating two failure modes

Appendix A

Nomenclature

σ	-	Total stress
σ_s	-	Stress experienced by spring
σ_d	-	Stress experienced by damper
ε	--	Total strain
ε_s	-	Strain in spring
ε_d	-	Strain in damper
μ	-	Dynamic viscosity
$\dot{\varepsilon}$	-	Strain rate
η	-	Kinematic viscosity
K	-	Spring stiffness
τ	-	Shear stress experienced by MTs
β	-	Angle between MTs and tau proteins
A	-	Projected area of MTs
R_O	-	Outer Radius of MT
R_i	-	Inner Radius of MT
d_T	-	Tau protein spacing
$\dot{u}_i$	-	Elongation of MT
α	-	Value corresponding to MT arrangement
U_i	-	Non dimensionalized MT elongation

Appendix B

Matlab script used for plotting

The following script is used to plot Tau protein elongation and MT strains shown in figures 4-1 to 4-4. By changing the length L value response was obtained for different lengths of MTs.

```
clear all
clc
%-------------------------------------------------------------------------
---%
t=35e-3;
T=0.1;
L=1e-6;%microm******************change of length*********************
Ro=12.5e-9;%nm
Ri=7e-9;%nm
Em=1.9e9;%Gpa
K=0.25e-3;%N/m
mu=70;
alpha=6;
beta=60;%deg
%dM=20e-9;%nm not used
dT=60e-9;%nm
%-------------------------------------------------------------------------
---%
Lc= sqrt((pi*(Ro^2-Ri^2)*dT*(Em+mu/t))/(2*alpha*K*0.5))
ee=0.001;%can change to diff vals later
x=0:0.000001:1;
%-----------------------------------------------------%
aa=Lc/(L*sqrt((ee/T)+1));
si=T/(1+((2*aa)*coth(1/(2*aa))));
u11a=si*(x+(aa*(sinh(x/aa)+(coth(1/(2*aa))*(1-cosh(x/aa))))));
u21a=(si*(x-(aa*(sinh(x/aa)+(coth(1/(2*aa))*(1-cosh(x/aa)))))))+T-si;

du11a=si*(1+(cosh(x/aa))-(coth(1/(2*aa))*sinh(x/aa)));
%------------------%
ee = 0.1;
aa=Lc/(L*sqrt((ee/T)+1));
si=T/(1+((2*aa)*coth(1/(2*aa))))
u12a=si*(x+(aa*(sinh(x/aa)+(coth(1/(2*aa))*(1-cosh(x/aa))))));
u22a=(si*(x-(aa*(sinh(x/aa)+(coth(1/(2*aa))*(1-cosh(x/aa)))))))+T-si;

du12a=si*(1+(cosh(x/aa))-(coth(1/(2*aa))*sinh(x/aa)));
%------------------%
ee = 1;
aa=Lc/(L*sqrt((ee/T)+1));
si=T/(1+((2*aa)*coth(1/(2*aa))))
u13a=si*(x+(aa*(sinh(x/aa)+(coth(1/(2*aa))*(1-cosh(x/aa))))));
u23a=(si*(x-(aa*(sinh(x/aa)+(coth(1/(2*aa))*(1-cosh(x/aa)))))))+T-si;

du13a=si*(1+(cosh(x/aa))-(coth(1/(2*aa))*sinh(x/aa)));
%------------------%
ee = 8;
```

```
aa=Lc/(L*sqrt((ee/T)+1));
si=T/(1+((2*aa)*coth(1/(2*aa))))
u14a=si*(x+(aa*(sinh(x/aa)+(coth(1/(2*aa))*(1-cosh(x/aa))))));
u24a=(si*(x-(aa*(sinh(x/aa)+(coth(1/(2*aa))*(1-cosh(x/aa)))))))+T-si;

du14a=si*(1+(cosh(x/aa))-(coth(1/(2*aa))*sinh(x/aa)));
%------------------%
ee = 15;
aa=Lc/(L*sqrt((ee/T)+1));
si=T/(1+((2*aa)*coth(1/(2*aa))))
u15a=si*(x+(aa*(sinh(x/aa)+(coth(1/(2*aa))*(1-cosh(x/aa))))));
u25a=(si*(x-(aa*(sinh(x/aa)+(coth(1/(2*aa))*(1-cosh(x/aa)))))))+T-si;

du15a=si*(1+(cosh(x/aa))-(coth(1/(2*aa))*sinh(x/aa)));
%-----------------------------------------------------------------------
---%
figure
plot(x,u21a-u11a,x,u22a-u12a,x,u23a-u13a,x,u24a-u14a,x,u25a-
u15a,'Linewidth',3)
I = legend( '$\eta\dot{\epsilon}$ = 0.001', '$\eta\dot{\epsilon}$ =
0.1','$\eta\dot{\epsilon}$ = 1','$\eta\dot{\epsilon}$ =
8','$\eta\dot{\epsilon}$ = 15');
set(I,'interpreter','latex');
title('Tau Protein elongation vs Scaled Length for Short
MTs','FontWeight','bold','FontSize',16,'FontName','Times New Roman');
xlabel('X','FontWeight','bold','FontSize',16,'FontName','Times New
Roman');
ylabel('Tau Protein
Elongation','FontWeight','bold','FontSize',16,'FontName','Times New
Roman');
grid on;
%---------------------%
figure
plot(x,du11a,x,du12a,x,du13a,x,du14a,x,du15a,'Linewidth',3)
I = legend( '$\eta\dot{\epsilon}$ = 0.001', '$\eta\dot{\epsilon}$ =
0.1','$\eta\dot{\epsilon}$ = 1','$\eta\dot{\epsilon}$ =
8','$\eta\dot{\epsilon}$ = 15');
set(I,'interpreter','latex');
title('Maximum MT strain vs Scaled Length for Short
MTs','FontWeight','bold','FontSize',16,'FontName','Times New Roman');
xlabel('X','FontWeight','bold','FontSize',16,'FontName','Times New
Roman');
ylabel('MT axial
strain','FontWeight','bold','FontSize',16,'FontName','Times New
Roman');
grid on;
```

References

1. Adnan, A., Qidwai, S., & Bagchi, A. (n.d.). Prediction of viscoelastic properties of microtubules via atomistic simulations. *In submission*.

2. Ahmadzadeh, H., Smith, D. H., & Shenoy, V. B. (2014). Viscoelasticity of tau Proteins leads to strain rate-dependent breaking of microtubules during axonal stretch injury: predictions from a mathematical model. *Biophysical journal*, 1123-1133.

3. Bliston, L. E., Liu, Z., & Phan-Thien, N. (1997). Linear viscoelastic properties of bovine brian tissue in shear. *Biorheology*, 377-385.

4. Brady, S., Siegel, G., Albers, R. W., & Price, D. (2005). *Basic neurochemistry: molecular, cellular and medical aspects.* Academic Press.

5. Davis, A. E. (2000, November). Mechanisms of Traumatic Brain Injury: Biomechanical, Structural and Cellular considerations . *Critical Care Nursing Quarterly*, pp. 1-13.

6. Frieden, T. R., Houry, D., & Baldwin, G. (2014). *Traumatic Brain Injury in United States: Epidemiology and Rehabilitation.* Atlanta: Center for Disease Control and Prevention.

7. Gennarelli, T. A. (1992). Mechanisms of brain injury. *The Journal of emergency medicine*, 5-11.

8. Holbourn, A. H. (1943). Mechanics of head injuries. *The Lancet*, 438-441.

9. Janmey, P. A., Euteneuer, U., Tarub, P., & Schliwa, M. (1991). Viscoelastic properties of vimentin compared with other filamentous biopolymer networks. *The Journal of cell biology*, 155-160.

10. Lewis, T. (2015, March 26). *Human Brain Facts, Anatomy & Mapping Project*. Retrieved from livescience: http://www.livescience.com/29365-human-brain.html

11. Lin, Y. C., Koenderink, G. H., Mackintosh, F. C., & Weithz, D. A. (2007). Viscoelastic properties of microtubule networks. *Macromolecules*, 7714-7720.

12. Nakagawa, A., Manley, G. T., Gean, A. D., Ohtani, K., Armonda, R., Tsukamoto, A., & Tominaga, T. (2011). Mechanisms of primary blast-induced traumatic brian injury: insights from shock-wave research. *Journal of neurotrauma*, 1101-1119.

13. Nicolle, S., Lounis, M., willinger, R., & Palierne, J. F. (2004). Shear linear behavior of brain tissue over a large frequency range. *Biorheology*, 209-223.

14. Ouyang, H., Nauman, E., & shi, R. (2010). Contribution of cytoskeletal elements to the mechanical property of axons. *Micro/Nano Symposium(UGIM)* (pp. 1-5). IEEE.

15. Reilly, P., & Bullock, R. (1998). Head Injury: Pathophysiology and Management of Severe Closed Injury. *European Journal of Emerging Medicine*, 367-368.

16. Smith, D. H., & Meaney, D. F. (2000). Axonal damage in traumatic brain injury. *The neuroscientist*, 483-495.

17. Smith, D. H., wolf, J. A., Lusardi, T. A., Lee, V. M., & Meaney, D. F. (1999). High tolerance and delayed elastic response of cultured axons to dynamic stretch injury. *The Journal of neuroscience*, 4263-4269.

18. Stalhammar, D. A. (1990). The mechanism of brain injuries. *Handbook of Clinical Neurology*, 17-41.

19. Stuhmiller, J. H., Phillips, Y. Y., & Richmond, D. R. (1991). The physics and mechanisms of primary blast injury. In *Converntional Warfare: Ballistic, Blast and Burn Injuries* (pp. 241-270). Washington DC.

20. Tang-Schomer, M. D., Johnson, V. E., Baas, P. W., Stewart, W., & Smith, D. H. (2012). Partial interruption of axonal transport due to microtubule breakage accounts for the formation of periodic varicosities after traumatic axonal injury. *Experimental neurology*, 364 - 372.

21. Tang-Schomer, M. D., Patel, A. R., Baas, P. W., & Smith, D. H. (2010). Mechanical breaking of microtubules in axons during dynamic stretch injury underlies delayed elasticity, microtubule disassembly, and axon degeneration. *The FASEB Journal*, 1401-1410.

22. Teasdale, G., & Bryan, J. (1974). Assessment of coma and impaired consciousness: a practical scale. *The Lancet*, 81-84.

23. Wegmann, S., Scholer, J., Bippes, C. A., Mandelkow, E., & Muller, D. J. (2011). Competing interactions stabilize pro-and anti-aggregant conformations of human Tau. *Journal of Biological Chemistry*, 20512-20524.

24. Wright, R. M. (2012, January). A Computational Model for Traumatic Brain Injury based on Axonal Injury Criterion. Baltimore, Maryland, USA.

25. Zink, E. k., & McQuillan, K. A. (2005). Managing Traumatic Brain Injury. *Nursing*, 36-43.

Biographical Information

Manikanta Jonnalagadda was born and raised in India. He graduated with First Honors degree in Aerospace Engineering from University of Hertfordshire. At UH, he worked with Dr. Andrew Lewis on Static divergence, Generic missile structure development. He also worked with Dr. Xu on Low velocity impact loading of composites. He pursued his Master of Science degree in Aerospace Engineering at University of Texas at Arlington. At the time, He worked with Dr. Ashfaq Adnan at Multiscale Mechanics and Physics lab, on Traumatic Brain Injury and the biomechanics involved at microscopic level.